LASER & PHOTONICS REVIEWS

www.lpr-journal.org

Silicon Multimode Waveguide Crossing Based on Anisotropic Subwavelength Gratings

*Weike Zhao, Xiaolin Yi, Yingying Peng, Long Zhang, Haitao Chen, and Daoxin Dai**

Multimode waveguide crossings (MWCs) are becoming more and more important as one of the key elements for on-chip optical routing and cross-connection. However, it is still very challenging to achieve scalable MWCs with compact footprints, low excess losses (ELs), and low intermode cross-talks (CTs). This work demonstrates an unprecedented silicon MWC with high performances by using the anisotropy of one-/two-dimensional (1D/2D) subwavelength grating (SWG) structures. For the proposed silicon MWC, the 2D-SWG crossing region at the center has a higher refractive index than the 1D-SWG regions at both sides for the guided-modes of TE polarization, due to the anisotropy of the 1D/2D SWGs. As a result, the crossing region can be equivalent to a straight waveguide, and the launched TE modes can transmit through the crossing region with negligible ELs and low intermode CTs. Such an MWC can be scaled very flexibly and easily according to the new principle. The fabricated three-mode MWC with a footprint of 14.8 × 14.8 μm^2 shows ELs of <0.26 dB and intermode CTs of <−20 dB in the wavelength range of 1525–1605 nm.

1. Introduction

Photonic integrated circuits (PICs) based on silicon-on-insulator (SOI) is deemed as one of the most promising platforms for the realization of on-chip optical interconnects because of the unique advantages of CMOS-compatibility and ultrahigh integration density.[1–4] On-chip mode-division-multiplexing has drawn tremendous attention as it is promising to further enhance the link capacity for a single wavelength carrier.[5,6] On the other hand, the realization of multimode photonic devices is usually very challenging because not only the fundamental mode but also the higher-order modes are involved. Great efforts have been made in recent years and fortunately some key multimode photonic devices have been successfully developed, including mode (de)multiplexers,[7–9] multimode power splitters,[10,11] multimode waveguide bends,[12–15] and multimode waveguide crossings (MWCs).[16–21]

Among them, low-loss and low cross-talk MWCs are becoming more and more important as one of the key elements for on-chip optical routing and cross-connection particularly for multimode PICs developed with increasing complexity. Currently, a few MWCs have been proposed by following the concepts of singlemode waveguide crossings.[22–25] For example, an MWC has been demonstrated by using a multimode interference (MMI) section whose length is chosen optimally as the common self-imaging length for all the mode channels.[16] The design is proposed by combining a pair of mode (de)multiplexers and multiple singlemode waveguide crossings.[17–18] However, these devices suffer a large footprint beyond 34 × 34 μm^2 and relatively high ELs of ≈0.9 dB.[18] By using the inverse design method to shorten the length of the MMI coupler, a compact two-mode MWC with a footprint of only 4.8 × 4.8 μm^2, ELs of 0.6 dB, and CTs of ≈−24 dB has also been demonstrated,[19] which however is hard to accommodate more mode channels. Recently, a star MWC has also been proposed with a novel Maxwell's fisheye lens structure which has a gradient index profile at the crossing center.[20,21] This two-channel MWC works well with ELs of ≈0.5 dB and CTs of ≈−20 dB in experiments.[20] However, partial truncation or gray-scale electron-beam lithography is needed for the fabrication of the structure with a gradient index profile. In short, it is still challenging to realize high-performance MWCs enabling more mode channels.

Metamaterials have attracted a lot of attention because it provides a flexible approach to control the flow of light[26,27] including one-dimensional (1D) and two-dimensional (2D) subwavelength structures. In particular, subwavelength gratings (SWGs) have been widely used in silicon photonics for some special on-chip mode and polarization manipulation.[28] The refractive-index contrast for optical waveguides can be modified by simply changing the duty cycle of the SWG, and thus various functional elements have been developed, including high-efficiency chip-fiber edge-couplers with a large fabrication tolerance, and low-phase-error multimode interferometers.[11,29–31] Furthermore, ultracompact mode converters and multimode waveguide bends have also been demonstrated by locally

W. Zhao, X. Yi, Y. Peng, L. Zhang, H. Chen, D. Dai
State Key Laboratory for Modern Optical Instrumentation
College of Optical Science and Engineering, International Research Center for Advanced Photonics, Zhejiang University
Zijingang Campus, Hangzhou 310058, China
E-mail: dxdai@zju.edu.cn

W. Zhao, D. Dai
Ningbo Research Institute
Zhejiang University
Ningbo 315100, China

The ORCID identification number(s) for the author(s) of this article can be found under https://doi.org/10.1002/lpor.202100623

DOI: 10.1002/lpor.202100623

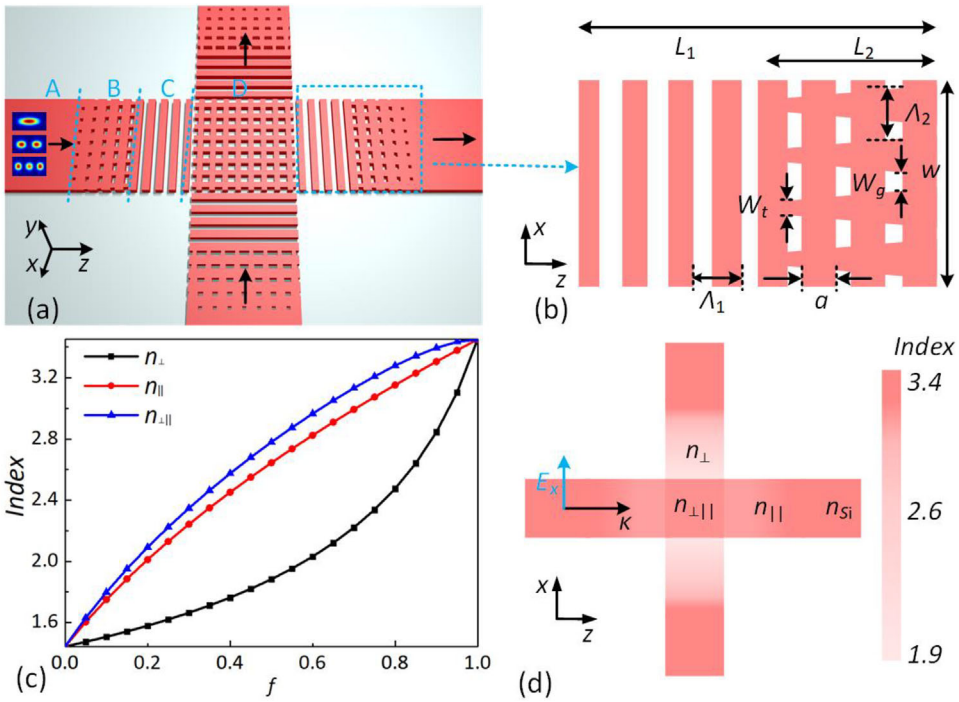

Figure 1. Schematic diagram of the proposed multimode waveguide crossing (MWC). a) 3D view; b) enlarged view for regions B and C; c) equivalent indices $n_\perp$, $n_{||}$, and $n_{\perp||}$ calculated by the effective medium theory (EMT) as the duty-cycle f varies. d) Effective index profile of the MWC for TE-polarization modes.

engineering the index profile of a single optical waveguide.[32–35] The anisotropy of SWGs is also advisable to develop high-performance polarization-handing devices, such as polarizers and polarization beam splitters.[36,37] In addition, ultrabroadband photonic devices with large fabrication tolerances have also been demonstrated by engineering the mode dispersion in SWGs.[38,39]

In this paper, we propose and demonstrate a novel MWC with unprecedented performances by using the anisotropy of 1D/2D SWG structures. The proposed silicon MWC has a 2D-SWG structure in the central crossing region and four 1D-SWG structures connected at the four ports. In this way, the MWC still behaves like a straight waveguide since the 2D-SWG crossing region at the center has a higher refractive index than the 1D-SWG regions at both sides due to the anisotropy of the 1D/2D SWGs. Therefore, the launched TE-polarization modes can transmit through the crossing region with negligible ELs and low intermode CTs. This is totally different from those waveguide crossings reported previously. The present three-mode MWC designed with a footprint of 14.8 × 14.8 μm^2 has ELs less than 0.15 dB and intermode CTs lower than −42 dB for all three guided-modes in an ultrabroad wavelength band of 1400–1700 nm theoretically. To the best of our knowledge, the proposed MWC shows the largest bandwidth with ultralow ELs and low intermode CTs. The fabricated three-mode MWC shows ELs of <0.26 dB and intermode CTs of <−20 dB in the wavelength range of 1525–1605 nm, which is limited by the bandwidth of the mode (de)multiplexers and the grating couplers. Furthermore, the proposed MWC can be scaled easily for working with more mode channels.

2. Structure, Principle, and Design

The present MWC is designed based on the SOI platform with a 220-nm-thick top-silicon layer (n_{Si} = 3.45), a 2-μm-thick silica buffer layer (n_{SiO2} = 1.444), as well as 2-μm-thick silica upper cladding. As shown in **Figure 1**a, the proposed MWC structure consists of two identical 1D-SWG waveguides crossed perpendicularly. As a result, a 2D-SWG structure is formed in the central crossing region (i.e., region D). For such an MWC, there are four 1D-SWG regions (region C), four adiabatic mode conversion sections (region B), and four regular input/output strip waveguide sections (region A). The 1D-SWG in region C and the 2D-SWG in region D are designed with a fixed period of Λ_1 in the longitudinal direction. In order to achieve the adiabatic transition from regions A to C, an adiabatic 2D-SWG with a lateral period of Λ_2 is introduced in region B [see Figure 1b], and the longitudinal duty cycle of the SWGs in regions B and C varies linearly from the maximum f_{Cmax} to the minimum f_{Cmin}.

According to the effective medium theory (EMT), an SWG structure can be treated approximately as a homogeneous waveguide made of equivalent birefringent materials and the refractive indices are given by[27,40–42]

$$n_{||}^2 = f n_{Si}^2 + (1-f)\, n_{SiO2}^2 \tag{1}$$

$$\frac{1}{n_\perp^2} = f\frac{1}{n_{Si}^2} + (1-f)\frac{1}{n_{SiO2}^2} \tag{2}$$

$$n_{\perp||}^2 = f n_{Si}^2 + (1-f)\, n_\perp^2 \tag{3}$$

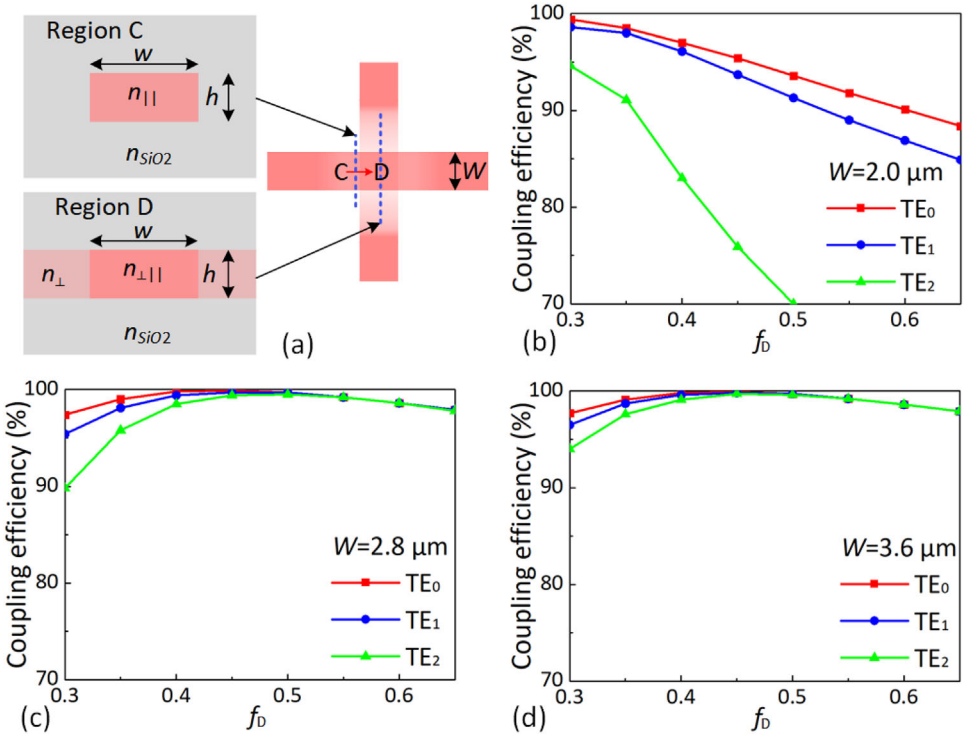

Figure 2. a) The cross-sections for the equivalent waveguide for the one-dimensional (1D) subwavelength grating (SWG) in region C as well as the equivalent waveguide for the two-dimensional (2D) SWG in region D; calculated mode coupling efficiencies for all three modes between the two equivalent waveguides as the duty cycle f_D varies from 0.3 to 0.65 for the cases with different core widths of $W = 2.0$ μm (b), 2.8 μm (c), and 3.6 μm (d).

where f is the longitudinal duty cycle of the SWGs, $n_{||}$ ($n_{\perp}$) is the equivalent index of the 1D-SWG waveguide for the polarization mode with a dominant electric field parallel (perpendicular) to the grating, and $n_{\perp||}$ is the equivalent index of the 2D-SWG structure in region D. Figure 1c shows the equivalent indices $n_{||}$, $n_{\perp}$, and $n_{\perp//}$ calculated with Equation (1) and one has $n_{\perp} < n_{||} < n_{\perp//}$. Note that there are some other formula to estimate the equivalent index of the 2D-SWG structure in region D[20,43–45] and the results are slightly different and still very similar. For the launched TE-polarization modes propagating along the z direction, the present MWC is then equivalent to a waveguide structure with a gradient index profile shown in Figure 1d. It can be seen that region D has a much higher equivalent index than region C at the lateral sides, indicating that light can propagate forward as guided modes and there is no much disturbation even though there is a waveguide crossing. This is totally different from those MWCs[16–21] reported previously. Here, we design a three-mode MWC as an example. The period is chosen as $\Lambda_1 = 200$ nm to guarantee the subwavelength-regime operation. Note that the EL for the proposed MWC mainly results from the transition loss at the junctions connecting different regions, as analyzed below.

Figure 2a shows the equivalent refractive indices $n(x, y)$ at the cross-section of the 1D-SWG waveguide in region C and the 2D SWG in region D. For region C (i.e., 1D-SWG waveguide), the core and the cladding have refractive indices of $n_{||}$ and n_{SiO2}, respectively. For region D (i.e., 2D SWG), the core and lateral cladding have refractive indices of $n_{\perp||}$ and $n_{\perp}$, respectively.

In order to achieve excellent mode confinement in both regions C and D, which is helpful to reduce the mode mismatch loss at the junction, we choose the duty cycle to be around 0.5 to maximize the refractive index contrast ($n_{\perp||}-n_{\perp}$). Meanwhile, the fabrication for SWG structures with a duty cycle around 0.5 is also relatively easy. Figure 2b-d shows the calculated mode coupling efficiencies between regions C and D as the duty cycle f_D in region D varies from 0.30 to 0.65. Here, the duty cycle f_{Cmin} in region C is fixed to be 0.5, while the waveguide width W is chosen as 2.0, 2.8, and 3.6 μm, respectively. When choosing a wider waveguide, the mode confinement becomes stronger and thus the coupling efficiency is expected to be higher, as shown in Figure 2b-d. For example, the waveguide core width is chosen as $W = 3.6$ μm to achieve high coupling efficiency. As shown in Figure 2d, when choosing $f_D = 0.45$, the mode coupling efficiencies are >99.7%, indicating that the mode mismatch loss is negligible. Furthermore, the mode coupling efficiencies for all three modes are higher than 99.2% when the duty cycle f_D varies from 0.4 to 0.5. It means that the coupling efficiency is not sensitive to the duty cycle. The large fabrication tolerance makes the present MWC very attractive.

In order to achieve adiabatic transition between regions A and D, the duty cycle f_C of the longitudinal 1D SWG in Regions B and C varies from the maximum f_{Cmax} to the minimum $f_{Cmin} = 0.5$ gradually with a length of L_1. Here, we choose $f_{Cmax} = 0.75$ because the minimal feature size allowed in the fabrication should be larger than 50 nm. For region B, the longitudinal period is chosen as $\Lambda_1 = 200$ nm, while the lateral period is given as $\Lambda_2 = W/N$, where W is the waveguide core width and N is the period number. The minimum gap w_g and the tip width w_t of the lateral SWG structure are chosen to 50 nm to minimize the

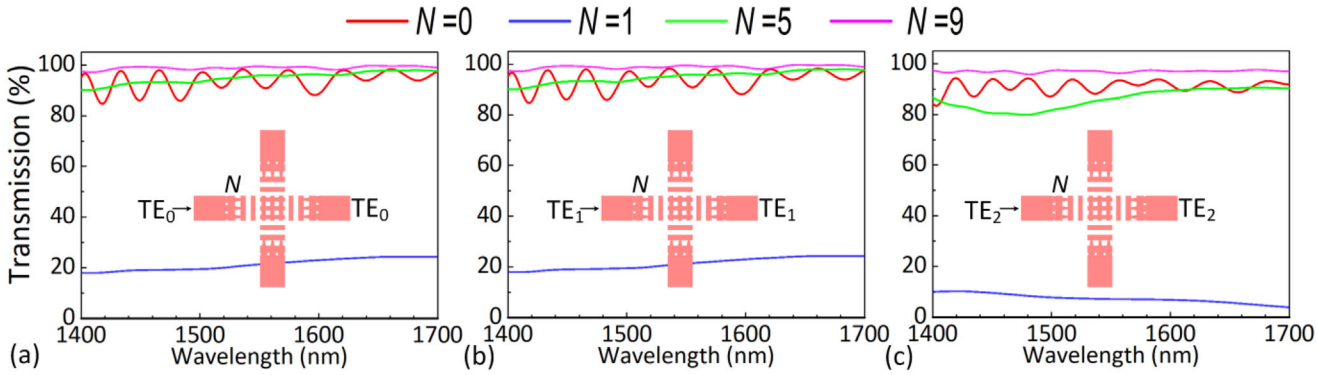

Figure 3. Simulated transmissions of the TE_0 (a), TE_1 (b), and TE_2 (c) modes in the present multimode waveguide crossing (MWC) with different lateral period numbers N. Here the parameters are $W = 3.6$ μm and $f_D = 0.45$.

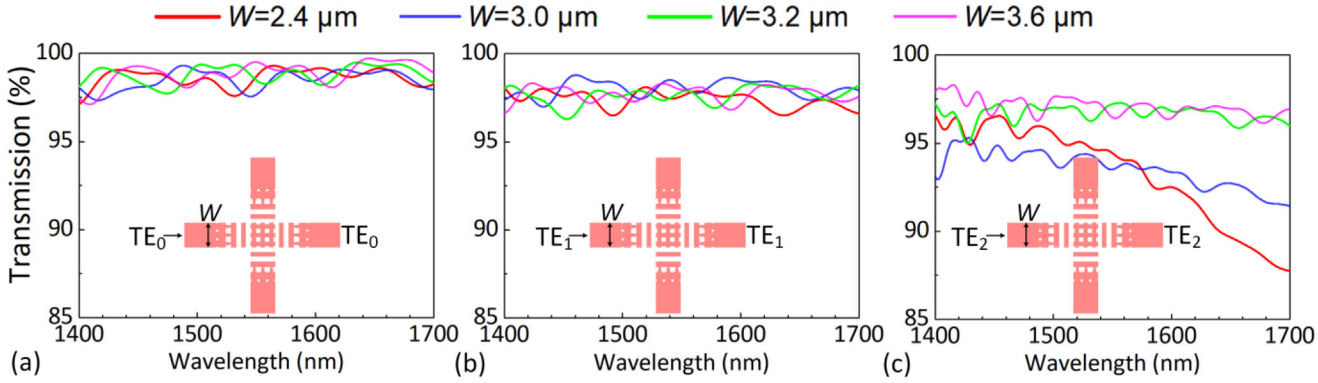

Figure 4. The simulated transmissions of the TE_0 (a), TE_1 (b), and TE_2 (c) modes in the present multimode waveguide crossing (MWC) with different waveguide widths W. Here the parameters are $f_D = 0.45$ and $N = 9$.

structure abruption. For Regions B and C, their lengths L_1 and L_2 are chosen to 5 and 2 μm, respectively, which are long enough to achieve adiabatic transition. **Figure 3**a-c shows the calculated transmissions of the proposed MWC for the TE_0, TE_1, and TE_2 modes, respectively, as the lateral period number N in region B varies. Here, a three-dimensional finite-difference time-domain (3D-FDTD) method is used for simulating the light propagation in the waveguide structures. From Figure 3a-c, it can be seen that the transmissions are strongly dependent on the lateral period number N. When $N = 0$, regions A and C are connected directly, and there is notable F-P resonance observed and the average transmissions are about 90%. When $N = 1$, region B becomes an SWG structure with a single longitudinal taper at the middle and there is huge mode mismatch at the junction between regions B and C, and consequently the average transmissions are less than 30%. Fortunately, when further increasing the period number, the transmissions increase and the F-P resonance becomes weak. According to the calculation results, the transmissions for all the TE_0, TE_1, and TE_2 modes are higher than 96.5% when choosing $N = 9$. One should note that the fabrication becomes more difficult with more periods due to the smaller feature size.

Moreover, we further check the transmissions of the TE_0, TE_1, and TE_2 modes in the present MWC when choosing different waveguide widths W, as shown in **Figure 4**a-c. For the TE_0 and TE_1 modes, transmission efficiencies higher than 96% are achieved even when the waveguide width W is smaller than 2.4 μm. However, for the TE_2 mode, the width W should be chosen to be larger than 3.2 μm so that the transmission is larger than 96.5%. Therefore, finally we choose $W = 3.6$ μm for the present design, and all key parameters of the designed MWC are summarized in **Table 1**.

Table 1. The key parameters of the designed multimode waveguide crossing (MWC).

Parameters	W [μm]	L_1 [μm]	L_2 [μm]	Λ_1 [nm]	Λ_2 [nm]	N	f_D	f_{Cmax}	f_{Cmin}
Value	3.6	5	2	200	400	9	0.45	0.75	0.5

For the designed MWC, light propagation of the launched TE_0, TE_1, and TE_2 modes (@1550 nm) are simulated by using the commercial software (3D FDTD, Lumerical), as shown in Figure 6a-c. It can be seen that all the TE_0, TE_1, and TE_2 modes go through the MWC with negligible ELs, and the present MWC performs just like a straight waveguide with slightly modulated refractive-index profiles. The output field profiles at the output end are also shown in **Figure 5**d-f, showing "perfect" field profiles for the TE_0, TE_1, and TE_2 modes.

Figure 6a-c shows the simulated transmission for the TE_0, TE_1, and TE_2 modes, respectively. It shows that the TE_0, TE_1, and TE_2

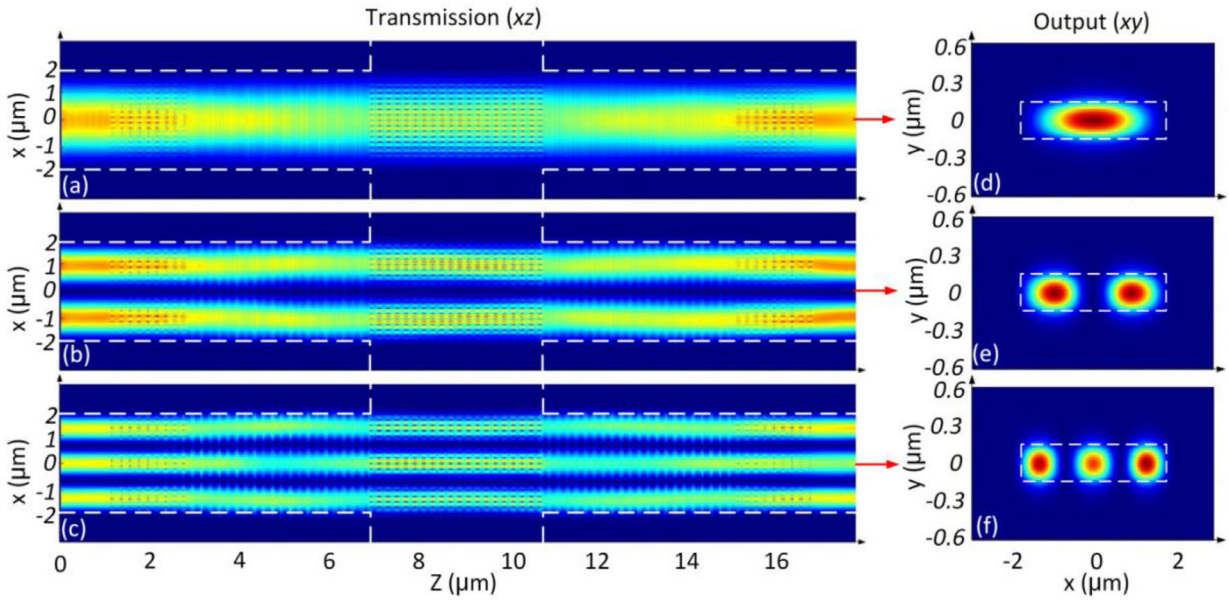

Figure 5. Simulated transmissions in the *xz* plane for the designed three-mode multimode waveguide crossing (MWC) when the TE_0 (a), TE_1 (b), and TE_2 (c) mode is launched, respectively. The field profiles at the output port are also shown in (d–f), respectively.

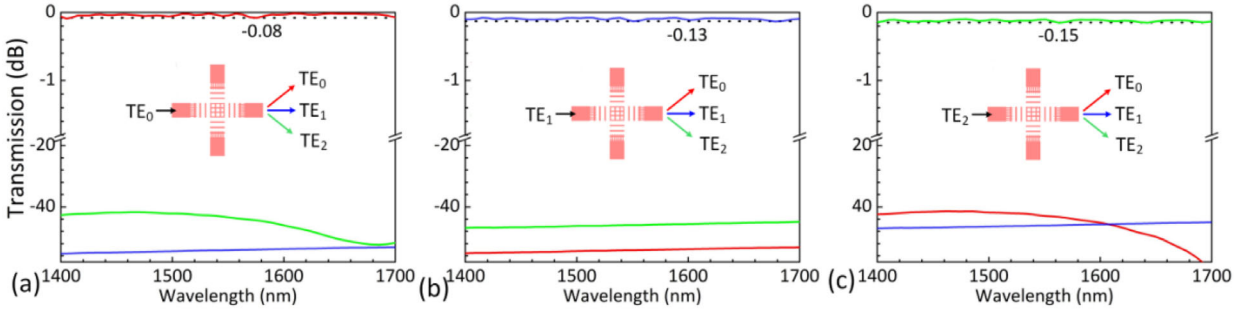

Figure 6. Simulated transmissions for the designed three-mode multimode waveguide crossing (MWC) with $W = 3.6$ μm when the TE_0 (a), TE_1 (b), and TE_2 (c) mode is launched, respectively.

modes have low ELs of <0.08, <0.10, and <0.15 dB in the ultra-broad wavelength band of 1400–1700 nm. The intermode CTs are as low as <−42 dB while the cross-talks to the crossing ports are less than −60 dB. As a comparison, an MWC consisting of two crossed strip waveguides with the same core width of $W = 3.6$ μm is also investigated, as shown in **Figure 7**a-c. It can be seen that the TE_0, TE_1, and TE_2 modes have high ELs of 0.15, 0.58, and 1.54 dB while the CTs are about −25 dB, which is much worse than the MWC presented in this paper. Predictably, the proposed MWC is very extensible and tolerant regardless of the mode

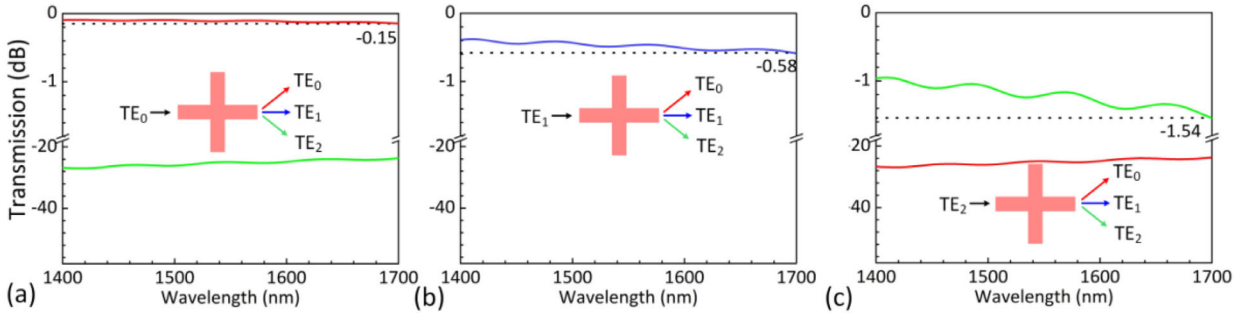

Figure 7. Simulated transmissions for the multimode waveguide crossing (MWC) consisting of two strip waveguides with $W = 3.6$ μm when the TE_0 (a), TE_1 (b), and TE_2 (c) mode is launched, respectively.

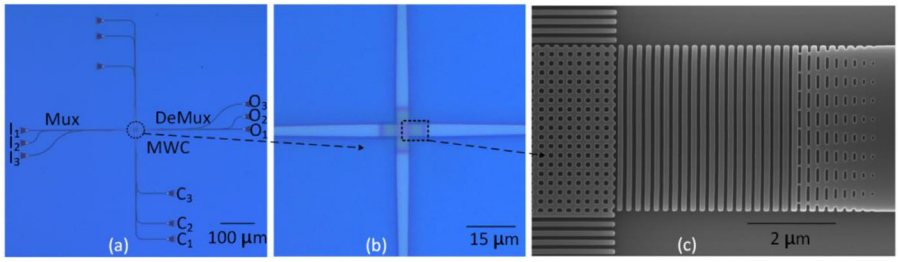

Figure 8. The microscopic images for the fabricated sample. a) The photonic integrated circuit (PIC) with an multimode waveguide crossing (MWC) and four mode (de) multiplexers; b) the enlarged view for the MWC; c) the scanning electron microscopy (SEM) image of the MWC.

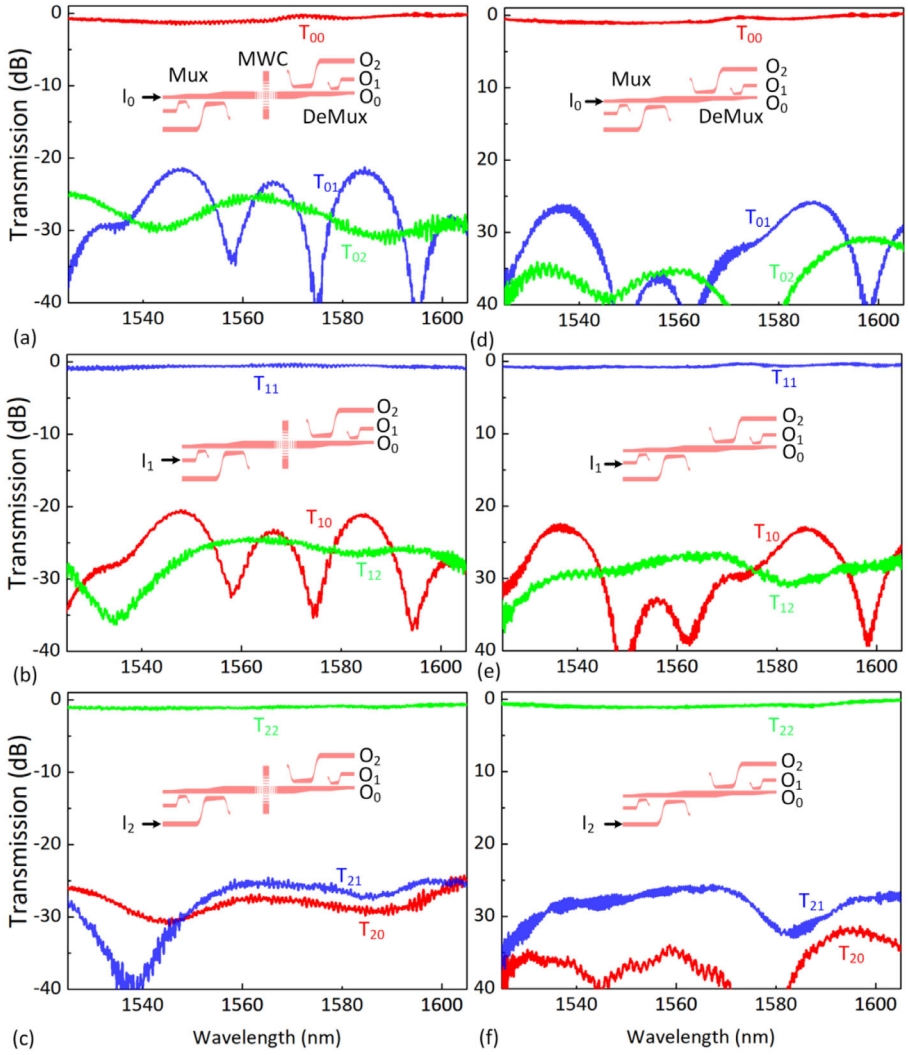

Figure 9. Normalized measurement transmissions T_{ij} for the photonic integrated circuit (PIC) with a pair of mode (de)multiplexers as well as the present multimode waveguide crossing (MWC) when the light is launched into I_0 (a), I_1 (b), and I_2 (c), respectively. Normalized measurement transmissions T_{ij} for the photonic integrated circuit (PIC) with a pair of mode (de)multiplexers when light is launched into I_0 (d), I_1 (e), and I_2 (f), respectively.

order and number because it performs as a straight waveguide due to the SWG hetero-anisotropy. As an example, a 10-mode MWC is further designed by simply increasing W from 3.8 to 12 μm to support the TE_0–TE_9 modes. The numerical simulation results show that all 10 modes have ELs less than ≈0.37 dB and CTs less than −19 dB in the wavelength range of 1450–1700 nm.

3. Experimental Section

The designed three-mode MWC was then fabricated with the fabrication process with E-beam lithography. The top-silicon layer and the buried-oxide layer are 220-nm thick and 2-μm thick, respectively. **Figure 8**a shows the microscopic image of the fabricated photonic integrated circuit (PIC), where there are four three-mode (de)multiplexers connected

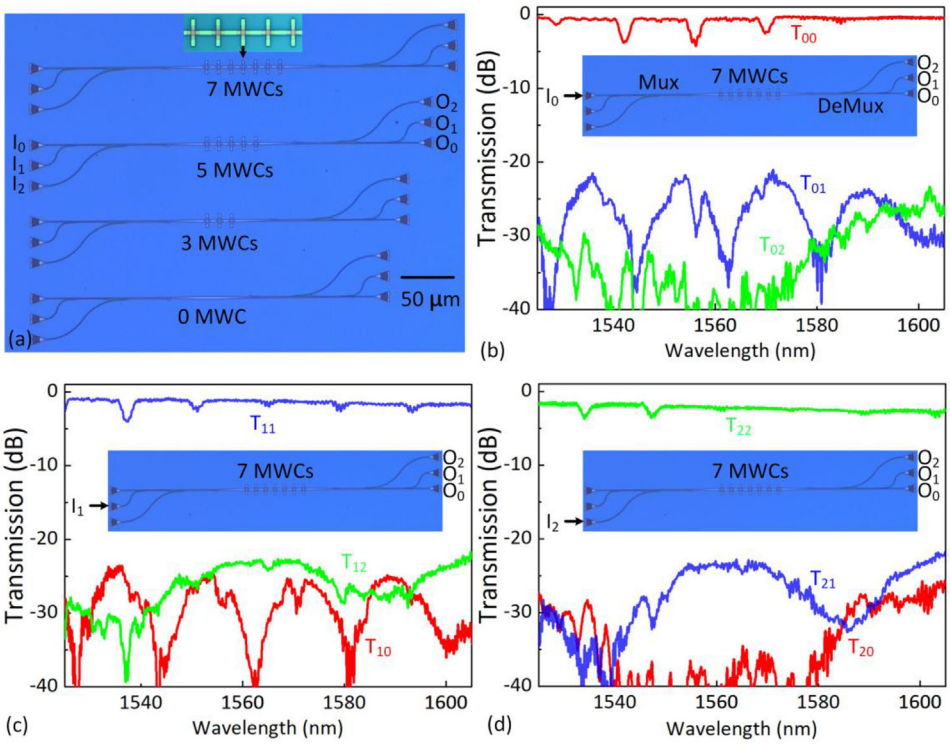

Figure 10. a) The microscopic image of the cascaded multimode waveguide crossings (MWCs) with $M = 0$, 3, 5, and 7. Normalized measurement transmissions T_{ij} for the photonic integrated circuit (PIC) with a pair of mode (de)multiplexers as well as seven MWCs when light is launched into port I_0 (b), I_1 (c), and I_2 (d), respectively.

to the four ports of the MWC. The mode (de)multiplexers based on dual-core adiabatic taper waveguides are used for mode (de)multiplexing in the characterization.[9] Grating couplers were used here for the fiber-chip coupling. Figure 8b shows the enlarged microscopic image for the part of MWC and Figure 8c shows the scanning electron microscopy (SEM) image of the fabricated MWC, showing the fabrication quality is pretty good.

For the characterization of the fabricated devices, an amplified spontaneous emission (ASE) light source was used and coupled to ports I_1, I_2, and I_3 through the grating couplers. In this way, the TE_0, TE_1, and TE_2 modes can be excited selectively. Meanwhile, light from the output ports (O_1, O_2, O_3) and the crossing ports (C_1, C_2, and C_3) are received through the corresponding grating couplers and characterized by an optical spectrum analyzer. The measurement results show that the crosstalks to the crossing ports (C_1, C_2, and C_3) are negligible (<−45 dB). Here, we show the measured transmission responses T_{ij} at output port O_j when light is launched from input port I_i. The measured results are shown in **Figure 9**a-c when the TE_0, TE_1, and TE_2 modes are excited, respectively. All these results are normalized with the transmission of the straight waveguide on the same chip. As a comparison, the transmission responses T_{ij} for the PIC with a pair of mode (de)multiplexers are shown in Figure 9d-f when the TE_0, TE_1, and TE_2 modes are excited, respectively. It can be seen that the fabricated mode (de)multiplexers work well with low ELs of ≈1.0 dB and low CTs of <−20 dB. For the PICs consisting of a pair of mode (de)multiplexers as well as the present MWC, the ELs for the three mode-channels are about 1.0 dB and the intermode CTs are less than −20 dB, which is similar to the results for the PIC with a pair of mode (de)multiplexers only. It indicates that the present MWC does not introduce notable ELs and intermode CTs.

In order to characterize the ELs of the MWC accurately, the testing structures with different numbers of MWCs in cascade were also fabricated on the same chip, as shown in **Figure 10**a. Here, the MWC number is chosen as $M = 0$, 3, 5, and 7. As an example, the measurement results for the case of $M = 7$ are given in Figure 10b-d, which shows the measured

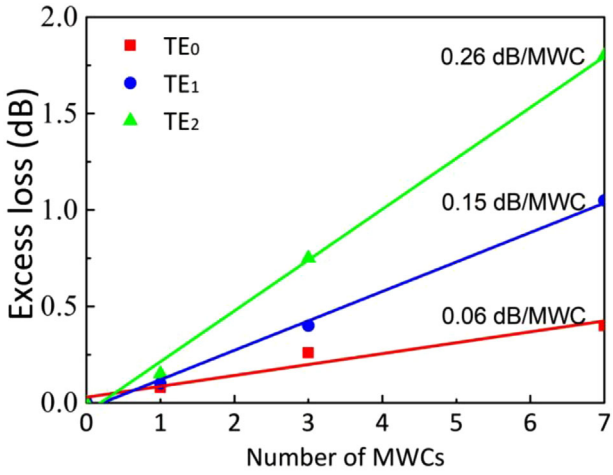

Figure 11. Measured average excess losses of the TE_0, TE_1, and TE_2 modes in the wavelength range of 1525–1605 nm for the cases with different multimode waveguide crossing (MWC) numbers, respectively.

transmission responses T_{ij} of the PIC with a pair of mode (de)multiplexers and seven MWCs for the launched TE_0, TE_1, and TE_2 modes, respectively. It can be seen that the intermode CTs are less than −20 dB, which is similar to the results for the PIC with a pair of mode (de)multiplexers only, also indicating that the present MWC does not introduce notable intermode CTs. Note that there are some resonant dips on the transmission spectra T_{ii} ($i = 0$, 1, 2), which is from the Fabry–Perot resonance due to some slight reflections in the MWCs. **Figure 11** shows the measured average excess losses in the wavelength range of 1525–1605 nm as the MWC number increases.

Table 2. Performance comparisons of silicon multimode waveguide crossings (MWCs).

Type	Mode channels	EL [dB]		CT [dB]		Bandwidth [nm]		Footprint [μm^2]
		Simul.	Exp.	Simul.	Exp	Simul.	Exp	
MMI couplers[16]	2	1.7	1.5	−32	−18	100 (EL < 1.7 dB, CT←32 dB)	80 (EL > 1.5 dB, CT←18 dB)	29 × 29
Asymmetric Y-Junction[18]	3	1.5	2	−22	−20	60 (EL < 1.5 dB, CT←22 dB)	60 (EL < 2 dB, CT←20 dB)	34 × 34
Inverse design[19]	2	0.5	0.6	−30	−24	80 (EL < 0.5 dB, CT←30 dB)	60 (EL < 0.6 dB, CT←24 dB)	4.8 × 4.8
Fisheye Lens[20]	2	0.3	0.5	−20	−20	100 (EL < 0.3 dB, CT←20 dB)	65 (EL < 0.5 dB, CT←20 dB)	18 × 18
Fisheye Lens[21]	3	1.14	≈2.68 @1550 nm	−21	−19.5 @1550 nm	400 (EL < 1.2 dB, CT←17 dB)	40 (EL = 5 dB, CT = −15 dB)	42 × 42
This work	3	0.15	0.26	−42	−20	300 (EL < 0.15 dB, CT←42 dB)	>80 (EL < 0.26 dB, CT←20 dB)	14.8 × 14.8
	10	<0.37	/	−19	/	250 (EL < 0.37 dB, CT←19 dB)	/	24 × 24

Here, the testing structure with five MWCs was broken and the data were unavailable. It can be seen that the average excess losses increases linearly as the MWC number increases. And the ELs for the TE_0, TE_1, and TE_2 modes are estimated to be ≈0.06, ≈0.16, and ≈0.26 dB per MWC. **Table 2** briefly summarizes the representative silicon MWCs reported until now. It can be seen that the present MWC shows the best performances with ultralow ELs, ultralow CTs, ultrabroad bandwidths, as well as compact footprints, which makes it attractive for developing multimode silicon photonics.

4. Conclusion

In summary, we have proposed and demonstrated an ultrabroadband MWC with ultralow losses, low cross-talks as well as compact footprints by using the anisotropy of 1D/2D SWG structures. In particular, there is a 2D-SWG structure in the central crossing region, and the SWG anisotropy enables a higher equivalent refractive index than the 1D-SWG structures locating at the lateral sides for the launched guided-modes of TE polarization. As a result, the crossing region still works as a straight waveguide supporting the ultralow-loss propagation of all the guided modes, which provides an unprecedented principle for realizing MWCs. A three-mode MWC has been designed and fabricated with a footprint of 14.8 × 14.8 μm^2. The ELs are <0.15 dB and the intermode CTs are <−42 dB for all three guided modes in an ultrabroad wavelength band of 1400–1700 nm in theory. The fabricated MWC has also shown very decent performances with low ELs of <0.26 dB and low intermode CTs of <−20 dB in the wavelength range of 1525–1605 nm (limited by the experimental setup). In addition, the proposed principle makes it very easy to be scaled to more mode channels. For example, a 10-mode MWC can be realized with ELs less than 0.36 dB and intermode CTs less than −19 dB for all the 10 modes in the wavelength range of 1450–1700 nm theoretically. Such a high-performance MWC is attractive and useful for developing multimode PICs in the future.

Acknowledgements

This project was supported by National Major Research and Development Program (No. 2019YFB2203604), National Science Fund for Distinguished Young Scholars (No. 61725503), National Natural Science Foundation of China (NSFC) (Nos. 61961146003, 91950205, 62005238, and 92150302), Zhejiang Provincial Major Research and Development Program (No. 2021C01199), Zhejiang Provincial Natural Science Foundation (No. LD19F050001), and the Fundamental Research Funds for the Central Universities.

Conflict of Interest

The authors declare no conflict of interest.

Data Availability Statement

The data that support the findings of this study are available from the corresponding author upon reasonable request.

Keywords

crossings, multimode, photonics, silicon, subwavelength grating

Received: November 1, 2021
Revised: February 4, 2022
Published online:

[1] R. Tkach, *Bell Labs Tech. J.* **2010**, *14*, 3.
[2] P. Dong, Y. Chen, G. Duan, D. Neilson, *Nanophotonics* **2014**, *3*, 215.
[3] M. Hochberg, T. Baehr-Jones, *Nat. Photonics* **2010**, *4*, 492.
[4] A. Shacham, K. Bergman, L. P. Carloni, *IEEE Trans. Comput.* **2008**, *57*, 1246.
[5] D. Dai, *Proc. IEEE* **2018**, *106*, 2117.
[6] C. Li, D. Liu, D. Dai, *Nanophotonics* **2018**, *8*, 227.

[7] T. Uematsu, Y. Ishizaka, Y. Kawaguchi, K. Saitoh, M. Koshiba, *J. Lightwave Technol.* **2012**, *3*, 2421.
[8] W. Chen, P. Wang, T. Yang, G. Wang, T. Dai, Y. Zhang, L. Zhou, X. Jiang, J. Yang, *Opt. Lett.* **2016**, *41*, 2851.
[9] D. Dai, C. Li, S. Wang, H. Wu, Y. Shi, Z. Wu, S. Gao, T. Dai, H. Yu, H.-K. Tsang, *Laser Photonics Rev.* **2017**, *12*, 1700109.
[10] H. Xu, Y. Shi, *Opt. Lett.* **2016**, *41*, 5047.
[11] C. Ye, M. Zhang, D. D. Dai, *Appl. Opt.* **2020**, *59*, 7308.
[12] L. Gabrielli, D. Liu, S. Johnson, L. Michal, *Nat. Commun.* **2012**, *3*, 1217.
[13] D. Dai, *Opt. Express* **2014**, *22*, 27524.
[14] X. Jiang, H. Wu, D. Dai, *Opt. Express* **2018**, *26*, 17680.
[15] C. Sun, Y. Yu, G. Chen, X. Zhang, *Opt. Lett.* **2017**, *42*, 3004.
[16] H. Xu, Y. Shi, *Opt. Lett.* **2016**, *41*, 5381.
[17] C. Sun, Y. Yu, X. Zhang, *Opt. Lett.* **2017**, *42*, 4913.
[18] W. Chang, L. Lu, X. Ren, L. Lu, M. Liu, M. Zhang, *IEEE Photonics J.* **2018**, *10*, 4501008.
[19] W. Chang, L. Lu, X. Ren, D. Li, Z. Pan, M. Cheng, D. Liu, M. Zhang, *Photonics Res.* **2018**, *6*, 660.
[20] H. Xu, Y. Shi, *Laser Photonics Rev.* **2018**, *12*, 1800094.
[21] S. Li, Y. Zhou, J. Dong, X. Zhang, E. Cassan, J. Hou, C. Yang, S. Chen, D. Gao, H. Chen, *Optica* **2018**, *5*, 1549.
[22] X. Li, H. Xu, X. Xiao, Z. Li, J. Yu, Y. Yu, *Opt. Commun.* **2012**, *312*, 148.
[23] P. Sanchis, P. Villalba, F. Cuesta, A. Hakansson, A. Griol, J. V. Galan, A. Brimont, J. Marti, *Opt. Lett.* **2019**, *34*, 2760.
[24] P. Bock, P. Cheben, J. Schmid, J. Lapointe, A. Delage, D. Xu, S. Janz, A. Densmore, T. Hall, *Opt. Express* **2010**, *18*, 16146.
[25] J. Feng, Q. Li, S. Fan, *Opt. Lett.* **2010**, *35*, 3904.
[26] L. Sun, Y. Zhang, Y. He, H. Wang, Y. Su, *Nanophotonics* **2020**, *9*, 13210.
[27] J. Luque-González, A. Sánchez-Postigo, A. Hadij-ElHouati, A. Ortega-Moñux, J. Wangüemert-Pérez, J. Schmid, P. Cheben, Í. Molina-Fernández, R. Halir, *Nanophotonics* **2021**, *10*, 2765.
[28] C. L. Li, M. Zhang, H. N. Xu, Y. Tan, Y. Shi, D. D. Dai, *PhotoniX* **2021**, *2*, 11.
[29] P. Cheben, J. H. Schmid, S. Wang, D. X. Xu, M. Vachon, S. Janz, J. Lapointe, Y. Painchaud, M. J. Picard, *Opt. Express* **2015**, *23*, 22553.
[30] P. Cheben, P. J. Bock, J. H. Schmid, J. Lapointe, S. Janz, D. X. Xu, A. Densmore, A. Delâge, B. Lamontagne, T. J. Hall, *Opt. Lett.* **2010**, *35*, 2526.
[31] A. Ortega-Monux, L. Zavargo-Peche, A. Maese-Novo, I. Molina-Fernández, R. Halir, J. G. Wangüemert-Pérez, P. Cheben, J. H. Schmid, *IEEE Photonics Technol. Lett.* **2011**, *23*, 1406.
[32] O. David, D. Boris, M. Noa, L. Uriel, *Nano Lett.* **2016**, *16*, 7956.
[33] Z. Li, M. H. Kim, C. Wang, Z. Han, S. Shrestha, A. Overvig, M. Lu, A. Stein, A. Agarwal, M. Lončar, N. Yu, *Nat. Nanotechnol.* **2017**, *12*, 675.
[34] J. Guo, C. Ye, C. Liu, M. Zhang, C. Li, J. Li, Y. Shi, D. X. Dai, *Laser Photonics Rev.* **2020**, *14*, 2000058.
[35] H. Wu, C. Li, L. J. Song, H. K. Tsang, J. E. Bowers, D. Dai, *Laser Photonics Rev.* **2019**, *13*, 1800119.
[36] H. Xu, D. X. Dai, Y. Shi, *Photonics Res.* **2019**, *7*, 1432.
[37] H. Xu, D. X. Dai, Y. Shi, *Laser Photonics Rev.* **2019**, *13*, 1800349.
[38] R. Halir, A. Maese-Novo, A. Ortega-Moñux, I. Molina-Fernández, J. G. Wangüemert-Pérez, P. Cheben, D. X. Xu, J. H. Schmid, S. Janz, *Opt. Express* **2012**, *20*, 13470.
[39] Y. He, Y. Zhang, Q. Zhu, S. An, R. Cao, X. Guo, C. Qiu, Y. K. Su, *J. Lightwave Technol.* **2018**, *36*, 5746.
[40] B. Vasić, G. Isić, R. Gajić, K. Hingerl, *Opt. Express* **2010**, *18*, 20321.
[41] J. Hunt, T. Tyler, S. Dhar, Y. Tsai, P. Bowen, S. Larouche, N. Jokerst, D. Smith, Planar, *Opt. Express* **2012**, *20*, 1706.
[42] R. Halir, P. Bock, P. Cheben, A. Ortega-Moñux, C. Alonso-Ramos, J. H. Schmid, J. Lapointe, D. Xu, J. G. Wangüemert-Pérez, I. Molina-Fernández, S. Janz, *Laser Photonics Rev.* **2015**, *9*, 25.
[43] B. G. Eric, M. G. Moharam, A. P. Drew, *J. Opt. Soc. Am. A* **1994**, *11*, 2695.
[44] X. Chen, H. K. Tsang, *Opt. Lett.* **2011**, *36*, 796.
[45] Y. Y. Tong, W. Zhou, X. R. Wu, H. K. Tsang, *IEEE J. Quantum Electron.* **2020**, *56*, 8400107.